

Supplemental Materials

Molecular Biology of the Cell

Rupprecht et al.

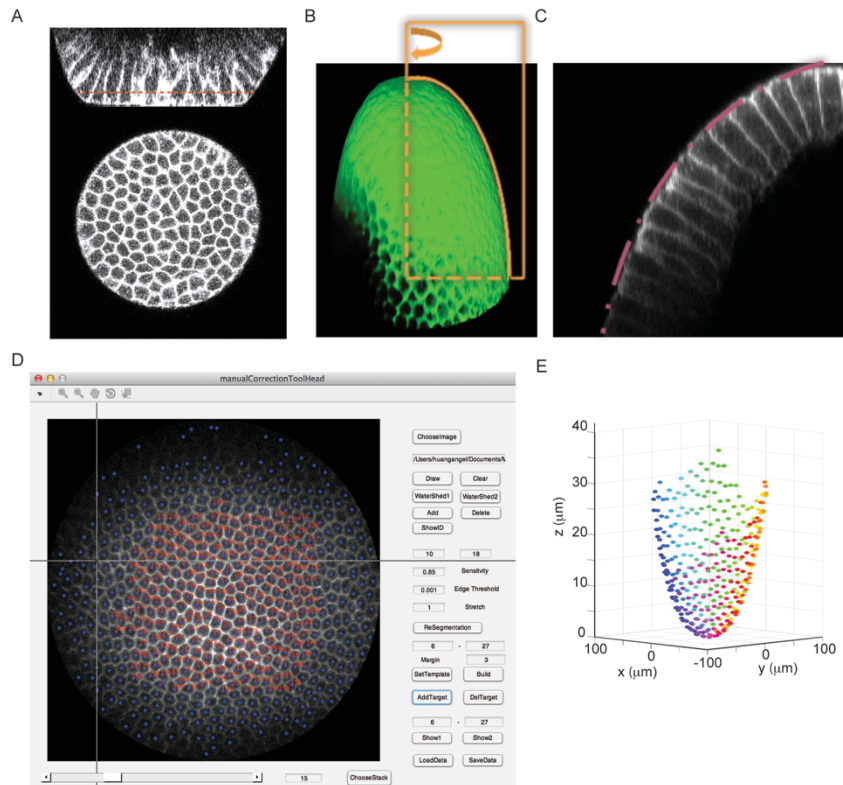
Supplementary Material for:

Geometric constraints alter cell arrangements within curved epithelial tissues

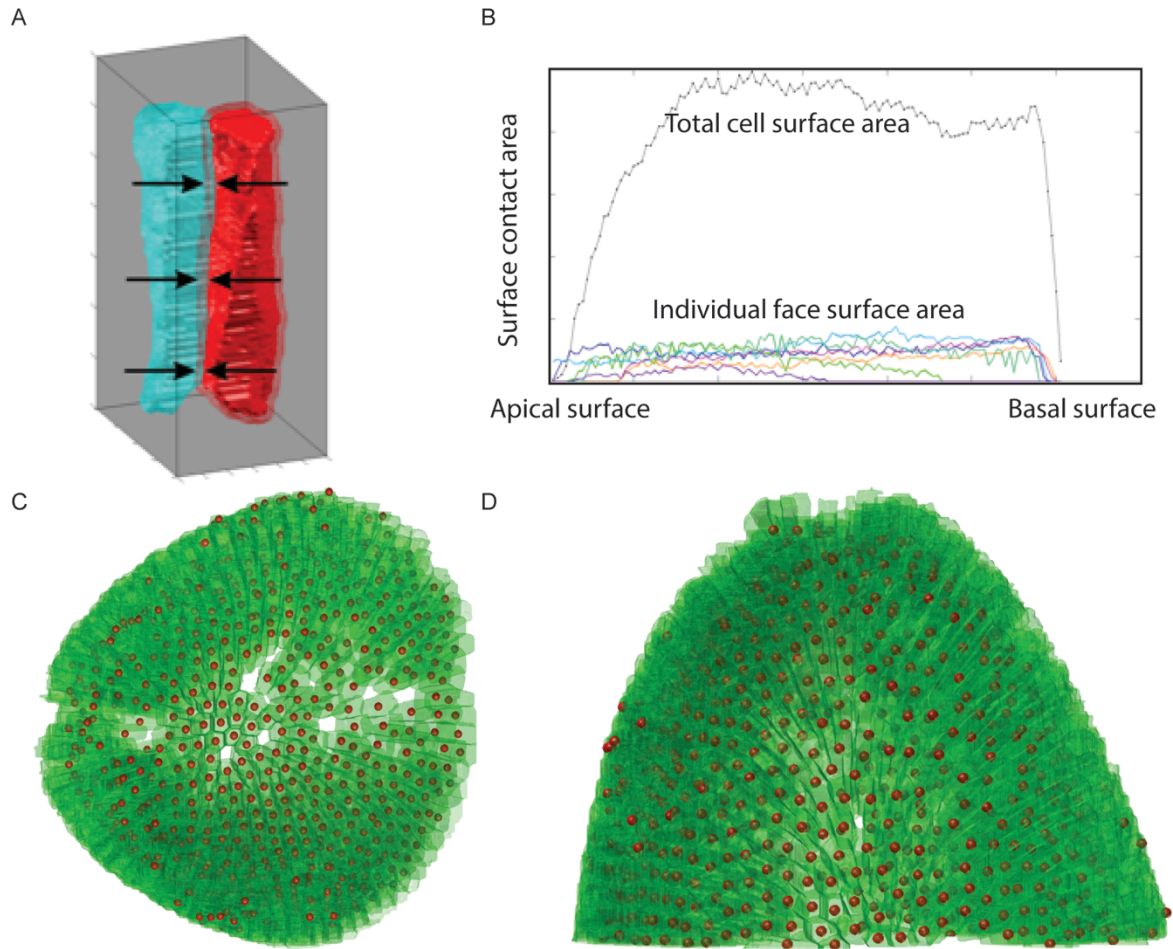
Jean-Francois Rupprecht, Kok Haur Ong, Jianmin Yin, Anqi Huang, Huy-Hong-Quan Dinh, Anand P. Singh, Shaobo Zhang, Weimiao Yu, Timothy E. Saunders

- 1. Supplementary Figures**
- 2. Supplementary Movies**
- 3. Image Analysis**
- 4. Further Theoretical Details**
- 5. Supplementary References**

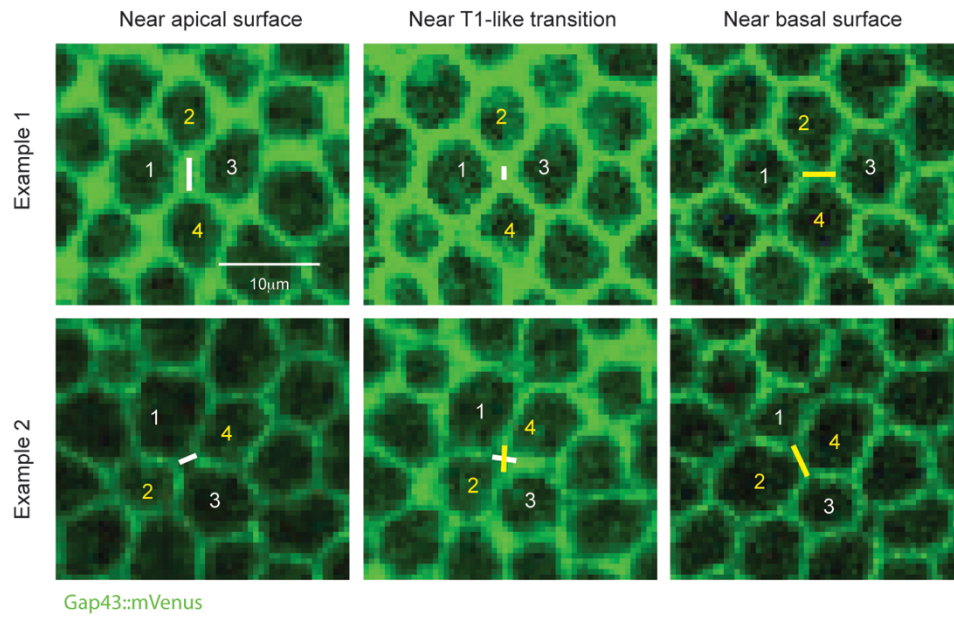
Supplementary Figures



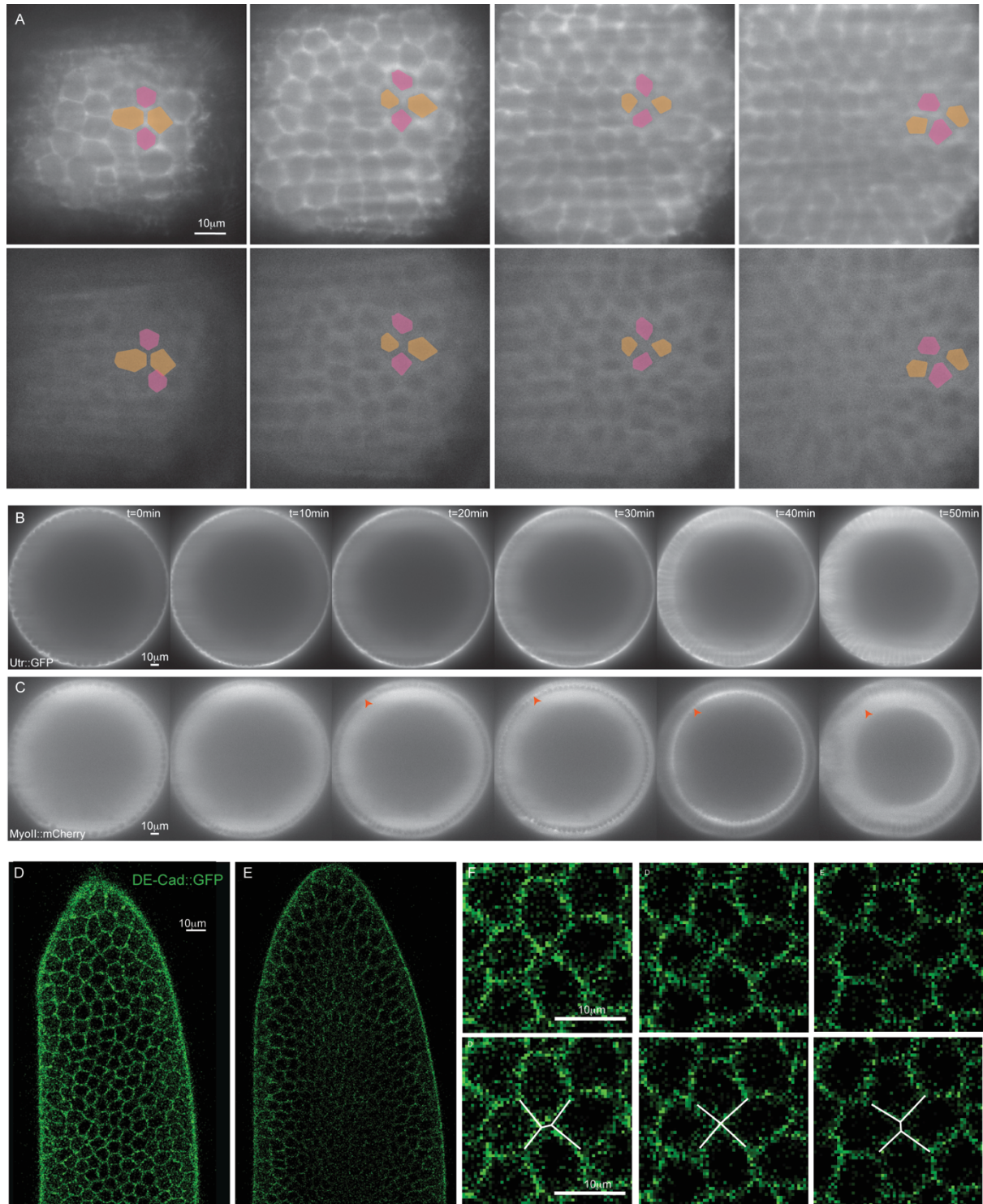
Supplementary Figure S1: Mounting and analyzing embryos along their anterior-posterior axis. A: Embryos that touch the cover slip show deformed anterior regions and alter cell structure. Top shows transverse view of embryo expressing Gap43::mVenus. Bottom shows plane touching the cover slip. The patterning and shape is clearly deformed compared to non-perturbed embryos. B: For each polar angle, the curve az^b is fitted to the embryo periphery (z denotes anterior to posterior axis), as described in Methods. C: The image is then projected onto the fitted curves for each angle to create flat planes for distances along the apical-basal axis of the cell, as shown in D. D: Computational framework for analyzing the projected images. Segmentation is performed using Matlab's Watershed algorithm. The user interface enables segmentation errors to be corrected and adjustment of seeds for each watershed iteration. The segmentation in one plane is used to seed the subsequent plane. E: The segmented data is then projected back into three-dimensions to ensure that there is no distortion due to the projection process.



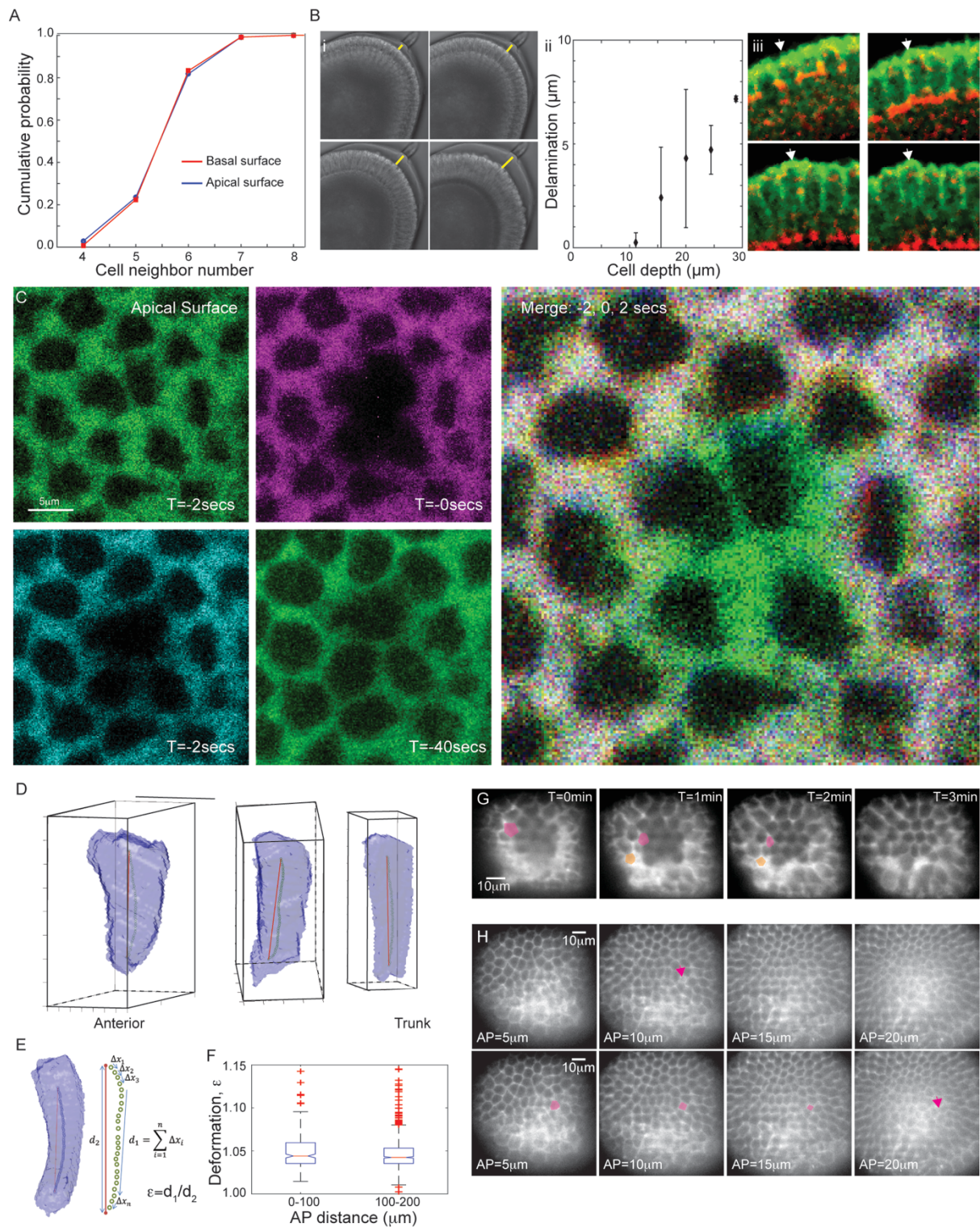
Supplemental Figure S2: Three-dimensional segmentation of light-sheet data and identification of cell rearrangements and cell orientation. A: After segmentation, two neighboring cells are dilated to measure overlap of neighboring areas to test for neighbor exchange. B: Quantification of the overlap area for a single cell with its six neighbors. Total surface area shown in black, which is used to identify the apical and basal surfaces. T1-transitions are identified by contact surfaces between neighboring cells reducing to zero between the apical and basal surface, e.g. light green curve in panel. C-D: View of segmented cells (denotes by red points) of an embryo along anterior-posterior axis (C) and laterally (D). White areas denote cells not successfully segmented. Green shading represents segmented cell volumes.



Supplemental Figure S3: Pseudo-T1 spatial transitions occur in the embryo trunk. Examples of pseudo-T1 spatial transitions in the trunk. The top example is the largest change in cell interface length observed in seven embryos. The bottom example is representative of most pseudo-T1 transitions observed in the trunk.



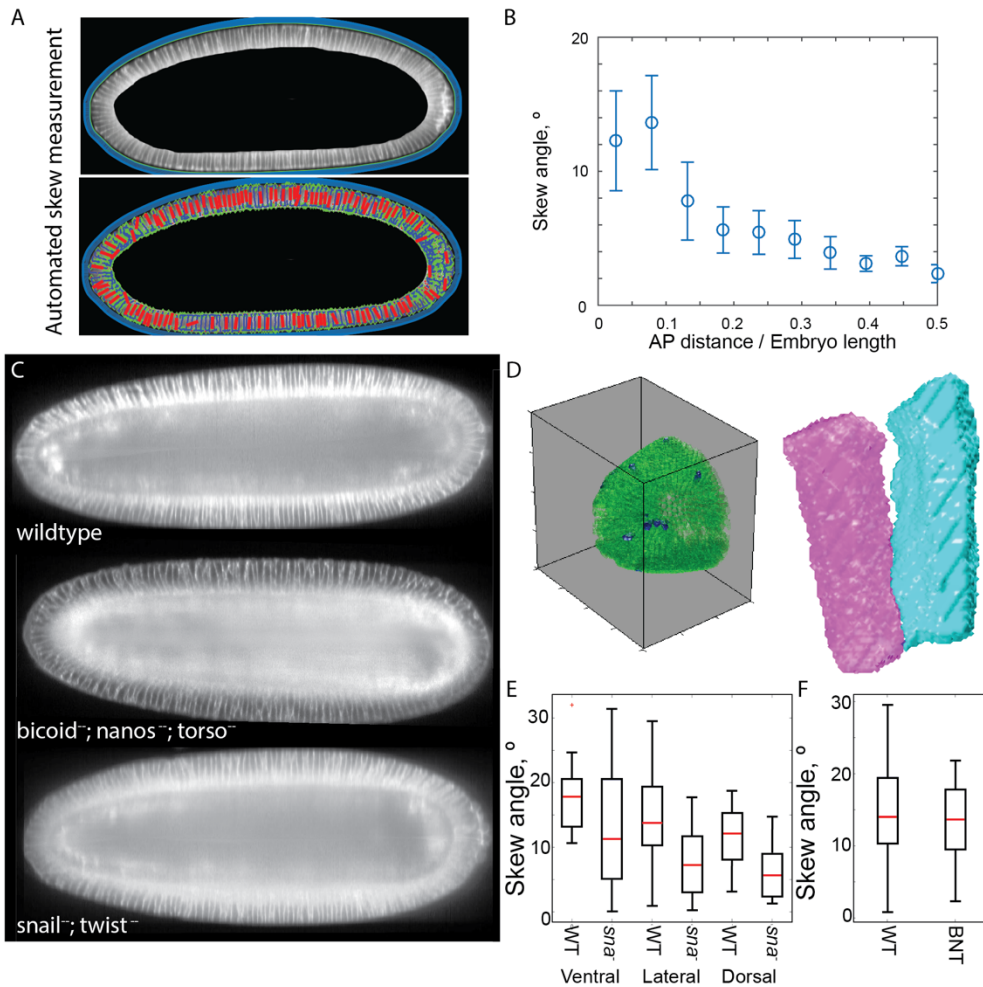
Supplemental Figure S4: Cellular rearrangements do not correlate with localization of MyosinII, Actin or DE-Cadherin. A: Embryo expressing Moe::GFP (top) and MyoII::mCherry (bottom) in the embryo anterior, imaged on a light-sheet microscope. Colored regions denote cells undergoing cellular rearrangements. B: Time lapse of embryo expressing Moe::GFP and (C) MyoII::mCherry at a fixed position from the anterior pole. Time t=0 min corresponds to around 10 minutes after mitotic division 13. D: Embryo expressing DE-Cadherin (DE-Cad) imaged on a light-sheet microscope, showing the trunk region. E: As (D) but showing cells more toward the anterior region. F: Cell rearrangement in the trunk region in embryo shown in D. No specific localization of DE-Cad is observed.



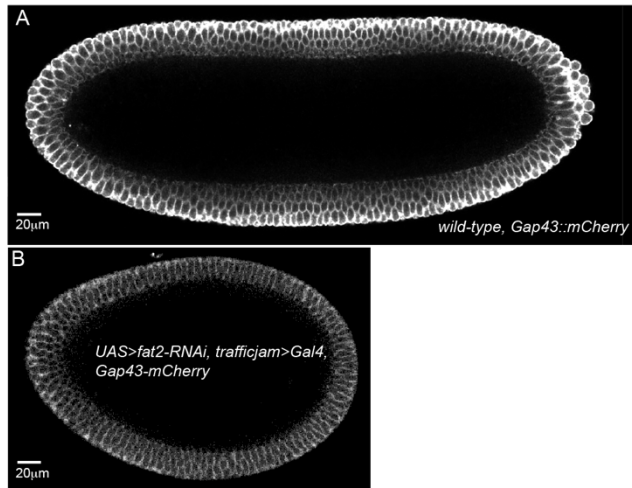
Supplemental Figure S5: Cell shape and mechanical properties under different perturbations.

A: The packing density is similar on both apical and basal surfaces in the anterior region ($n=8$ embryos, > 1000 cells). B: (i) In a subset of embryos ($\sim 25\%$), the anterior-most cells disassociate (akin to delamination) from the egg anterior. (ii) In such embryos ($n=4$), this delamination only occurs once the basal surface has invaginated greater than $15 \mu\text{m}$ from the apical surface. (iii) For cells that have delaminated, the apical surface appears soft, with blebbing-like behavior observed (denote by white arrowhead). C: Laser ablation of apical surface of embryo expressing Gap43::Venus. Ablation performed during cycle 14 as described in ¹. The four subpanels show the cell membranes before (-2secs), during (0secs) and after ($+2\text{secs}$, $+40\text{secs}$) ablation. Right panel shows the merged image for the -2secs , 0secs and $+2\text{secs}$ images. D: Examples of cells shapes in the anterior (left), around $80 \mu\text{m}$

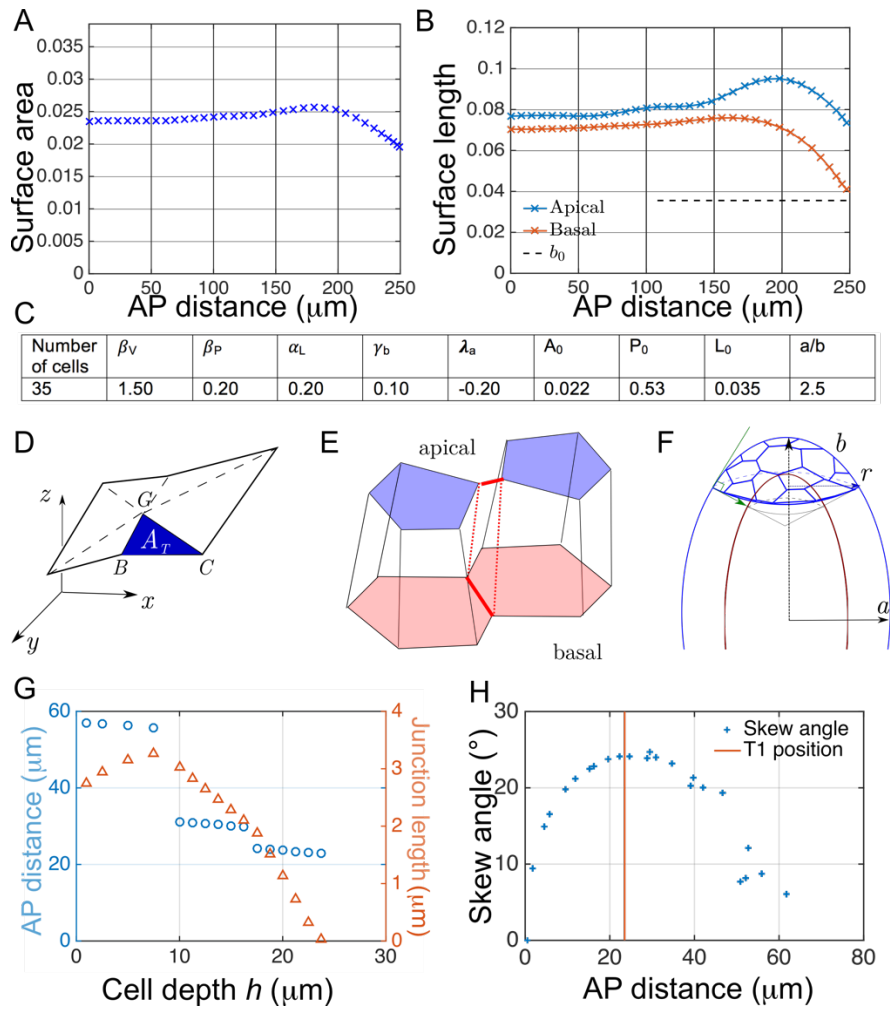
from the tip (center) and about 200 μm from the anterior tip. E: Quantification of cell deformation by comparing the linear apical-to-basal distance (d_2) with the curved distance along the cell centroid at each plane along the apical-basal axis (d_1). Deformation defined by $\varepsilon = d_1/d_2$. F: Comparison of ε from light-sheet data of embryos in late slow phase ($n=3$ embryos, > 500 cells) for cells closer than 100 μm to the anterior pole and cells toward the trunk. G: Time course of cell with restricted basal surface area, as shown in Figure 5G, here highlighting the change in cell shape. H: bcd^{E1} embryo expressing Gap43::mCherry. At fixed time point (beginning of fast phase) with different positions from the anterior pole shown. Magenta arrow highlights cells with reduced basal surface, with the shape of each such cell highlighted on the bottom row.



Supplemental Figure S6: Automated cellular skew measurements agree with manual analysis and comparison of cell rearrangements and cell skew in different genotypes. A: Automated analysis of cell skew. (Top) The embryo periphery is annotated manually and then the normal vector to the surface at each point is calculated. (Bottom) The cross-sectional view of each cell is segmented (using Ilastik²) and only those segmented with high quality are analyzed. The average orientation of the cell (denoted by orientation of red bar) is then used to calculate the angle of the cell relative to the embryo surface. B: Automated calculation of cellular skew (n=3 embryos). Absolute angles are taken (i.e. relative orientation ignored) and skew angles above 30° are filtered out as these are due to mis-segmentation (confirmed by visual inspection). C: *bicoid-nanos-torso-like* (*bnt*) (center) and *snail-twist* (bottom) embryos compared with wildtype (top). Embryos expressing Gap43::mCherry. D: Identification of pseudo-T1 transitions in *bnt* embryo (blue cells). Right shows two cells undergoing neighbor rearrangement along cell apical-basal axis in a *bnt* embryo. E: Boxplot comparison of skew angle in wildtype and *snail-twist* mutants (denoted by *sna*⁻) in the region within 50 μm of the anterior pole. F: As (E) but comparing the average skew for wild-type and *bnt* embryos.



Supplemental Figure S7: *fat2-RNAi* embryos are significantly more spherical than wild-type embryos. A: Wild-type embryo toward end of slow phase expressing Gap43-mCherry. B: UAS>*fat2-RNAi* driven by *trafficjam*>Gal4 embryos expressing Gap43-mCherry. Scale is same in (A) and (B).



Supplemental Figure S8: Vertex modeling of columnar cells in a curved environment. (A-C) 2D Vertex model. A: Cellular area is almost constant and equal to the preferred area $A_0 = 0.022$ (in unit of the embryo width b). The area is a proxy of the cell volume. B: Basal and apical lengths do not vary significantly close to the head. The basal length is always larger than the target length $L_0 = 0.035$, indicating that the basal regulation tends to contract the basal surface. C: Table of the parameters used to obtain the results presented in Figure 8 (main text). The parameters α_L , γ_b , λ_a control tension along the lateral, basal and apical edges, respectively; β_V and β_P represent the compressibility in area and perimeter of the simulated cells, which represent regulations of the biological cell volume and membrane area. A_0 , P_0 , L_0 represents preferred area, perimeter and basal length. Vertices on the apical side are constrained to move along an ellipse of main axis of length $a = 2.5$ and minor axis of length $b = 1$. (D-H) 3D Vertex model. D: Sketch of the face triangulation for area measurement. E: Sketch of an apical-basal T1 in our 3D vertex model. F: Sketch of the simulation region, here a cap of an ellipsoid of radius r . Green vector: the normal projection of an apical vertices along the normal to the ellipsoid. G: Length of the shortest cell junction on the apical axis (right orange axis) and AP distance of the shortest cell junction (left blue axis) as a function of the cell depth h . H: Cell skew (defined as the angle between the apical and basal vertices and the normal to the apical vertex) as a function of the AP distance. The maximum of the cell skew corresponds to the position of the first observed T1 transitions.

Supplementary Movies

Supplemental Movie S1: Z-plane imaging of *Drosophila* embryo in microfluidic device

Movie showing plane-by-plane a fixed *Drosophila* embryo in cycle 14 expressing H2Av::mCherry (red) and Gap43::mVenus (green), with the microfluidic chamber visible in grayscale.

Supplemental Movie S2: Stereographic projection of embryo anterior pole

Movie through the slices of the anterior pole after the stereographic projection of a fixed embryo expressing Gap43::mVenus in late slow phase. First frame corresponds to near apical surface. Last few frames correspond to basal surface. The anterior-most cells are slightly shorter than the other cells (hence dark region at end of movie in the center).

Supplemental Movie S3: Close up of segmented cells undergoing cellular rearrangements along apical-basal axis

Supplemental Movie S4: Laser ablation on cell apical surface

Laser ablation of *Drosophila* embryo expressing Gap43::mVenus toward end of slow phase. Ablation in trunk region. Refer to ¹ for detailed methods.

Supplemental Movie S5: *fat2-RNAi* embryo expressing Gap43-mCherry during cycle 14

UAS>*fat2-RNAi*, *trafficjam*>Gal4, Gap43::mCherry embryo through cycle 14. Orientated with anterior to left and ventral side at the bottom. Gastrulation appears to occur normally.

Supplemental Movie S6: 3D vertex model - apical junctions near the head

3D vertex model evolution of the apical junctions near the head – modeled as an ellipsoid geometry - during the cell depth relaxation phase: (left column) for a cell depth $h = 10 \mu\text{m}$, corresponding to an early phase during cellularization, and (right column) for a cell depth $h = 20 \mu\text{m}$; (upper rows) color coding represents neighbor number of each apical faces: green for hexagons, blue for pentagons, and yellow for heptagons. The apical T1 transitions that appear for $h = 20 \mu\text{m}$ units relax at long time scale. (lower rows) 3D tissue structure: apical (blue) and basal (red) networks.

Supplemental Movie S7: 3D vertex model – apical junctions near the trunk

As Supplementary Movie 6, but with a cylindrical geometry.

Image Analysis

Semi-automated three-dimensional embryo cell segmentation for light-sheet datasets

In our three-dimensional (3D) image preprocessing, the 3D cell image is first smoothed with a 3D Gaussian kernel with kernel size 7 voxels and $\sigma = 2$. This was then followed by enhancing image intensity with contrast adjustment in the fixed range [0.0, 0.1]. The enhanced image was then used to perform 3D cell segmentation with an iterative seeds-controlled watershed algorithm. The watershed algorithm³ is also known as region-based image segmentation approach. In our study, the 3D watershed algorithm is applied to segment the 3D cells semi-automatically, where the process flows involved human interaction to allocate seeds for the watersheds manually to improve the 3D cell segmentation iteratively.

Cell membrane morphology was extracted using a morphological opening process with a spherical kernel, and then contrast adjustment was employed to enhance the image intensity signal further for all cell membranes. This step generates the local maxima (seeds) for each cell region before segmentation with a watershed algorithm. In the post-processing, artefact noise introduced during the segmentation process was removed with using morphological operations.

Human interaction can improve the 3D cell segmentation because the membrane cell information is not always sufficient to identify entire local maxima. Hence, we utilized a binary image generated after the final process of the watershed algorithm as the reference to assign seeds. In this process, the binary image is superimposed on top of original image. Thus, we can identify the cell which is not segmented successfully in the previous iteration. Subsequently, the seed region is allocated using the freely available software package Medical Image Processing, Analysis and Visualization (MIPAV) (<https://mipav.cit.nih.gov/>). We employed automatic level set annotation tools available to draw the cell region to speed up the annotation process, and this annotated cell was then converted into the binary image as the 3D seeds image. In the final step, the annotated 3D seeds are combined with the previously identified seeds to re-perform the watershed algorithm and morphological operation to get the final 3D cell segmentation. Only cells with high confidence in segmentation (e.g. no large variation in cross-sectional area between planes) were analyzed.

Cell shape rotation

Standardizing each cell to lie perpendicular to the anterior-posterior plane of the embryo is necessary for the quantitative computation. Therefore, transformations for rotating each 3D cell to the axis along the anterior-posterior plane (z-axis) is performed⁴. In general, the rotation method for each 3D cell can be described as follows:

Step 1: Move the 3D cell to the origin of the 3D embryo.

Step 2: Rotate the 3D cell along the Z-axis(anterior-posterior) thus rotation axis stick to the XZ plane.

Step 3: Rotate the 3D cell along the Y-axis(superior-inferior) thus rotation axis stick to the Z-axis.

Step 4: Move back the 3D cell to its original position.

We define a 3D cell with it center mass (a,b,c) and vector (u,v,w) to anterior-posterior axis. The matrix to rotate a cell in a vector can be defined in following:

$$T_1 = \begin{bmatrix} 1 & 0 & 0 & 0 \\ 0 & 1 & 0 & 0 \\ 0 & 0 & 1 & 0 \\ -a & -b & -c & 1 \end{bmatrix}$$

$$R_{xz} = \begin{bmatrix} \frac{u}{\sqrt{u^2 + v^2}} & \frac{v}{\sqrt{u^2 + v^2}} & 0 & 0 \\ -\frac{v}{\sqrt{u^2 + v^2}} & \frac{u}{\sqrt{u^2 + v^2}} & 0 & 0 \\ 0 & 0 & 1 & 0 \\ 0 & 0 & 0 & 1 \end{bmatrix}$$

$$R_z = \begin{bmatrix} \frac{w}{\sqrt{u^2 + v^2 + w^2}} & \frac{v}{\sqrt{u^2 + v^2}} & 0 & 0 \\ -\frac{v}{\sqrt{u^2 + v^2}} & \frac{u}{\sqrt{u^2 + v^2}} & 0 & 0 \\ 0 & 0 & 1 & 0 \\ 0 & 0 & 0 & 1 \end{bmatrix}$$

$$T_2 = \begin{bmatrix} 1 & 0 & 0 & 0 \\ 0 & 1 & 0 & 0 \\ 0 & 0 & 1 & 0 \\ a & b & c & 1 \end{bmatrix}$$

$$tf = T_1 * R_{xz} * R_z * T_2$$

Where the transformation matrix is tf for 3D cell perpendicular to the anterior-posterior plane of the embryo, T_1 is translation to the origin of the embryo, R_{xz} is rotation to the XZ plane, R_z is rotation to the Z-axis and T_1 is translation back to its original position.

Pseudo-T1 transitions

The interaction between two cells are undergoing a pseudo-T1 transition can be visualized and identified using the 3D cell shapes. We reconstructed the 3D cluster (i.e. neighboring cells) for each cell from the output of the rotated 3D cell segmentation. Subsequently, we dilated (spherical kernel of 5 pixels) a cell of interest in the cluster to make it slightly larger to touch with the other cells nearby, see Supplemental Figure S2A. Thus, the overlap volume between neighboring cells can be measured along the apical-basal axis. These overlapping voxels can then be plotted for each different face (i.e. different neighbor overlaps), Supplemental Figure S2B. The black line in Supplemental Figure S2B shows the cell surface change of the dilated cell along the apical-basal axis.

Degree of cell deformation

To examine the effect of curvature on overall cell morphology we quantified the deformation of cells in the light-sheet data by comparing the ratio of the apical-basal distance (d_1) to the total curved distance of the cell from apical to basal surfaces (d_2). We used the measure $\epsilon = d_2/d_1$, where $\epsilon = 1$ for a straight cell and ϵ increases above 1 for non-columnar cells, Supplemental Figure S5, D-F. However, we did not see a significant difference in cell deformation between anterior and more centrally located cells. This could be due to difficulty in analyzing the light-sheet data. We only included cells segmented with high confidence. Imaging limitations of the light-sheet data in the anterior and the difficulty in segmenting highly deformed cells, meant that the data was biased toward only minimally deformed cells.

We computed the degree of deformation, as illustrated in Supplemental Figure S5, D-F. We calculated the Euclidean distance d_2 in between 15 percentile from the apical surface of the cell and 10 percentile from the basal surface of the cell. Subsequently, the Euclidean distance for Δx is calculated in between the center of mass of two slices which is interpolated in 3D space. The d_1 can be calculated with a summation of all Δx along the AP-axis of the cell:

$$d_1 = \sum_{i=1}^n \Delta x_i,$$

where n denotes the total number of steps taken along the apical-basal axis. Lastly, ϵ is then computed as defined in Supplemental Figure S5E, where $\epsilon = 1$ is indicated a straight cell and $\epsilon > 1$ represents the degree of deformation of the cell.

Additional Theoretical Notes

Cell packing density

In a perfectly flat system, we expect the packing density to be 6 – i.e. all cells hexagonal. On a sphere, for example a football, then the packing density decreases ~ 5.7 due to the additional 12 pentagons (the precise change depends on the number of faces). Approximating the anterior pole as a hemisphere, we require the addition of 6 pentagons to satisfy the Euler conditions. So, taking ~ 100 cells in the head region, then we expect the packing density to be $94/100 * 6 + 6/100 * 5 = 5.94$, which is $\sim 1\%$ variation from 6. But the packing error even in flat tissues is larger than this. So, we do not expect to be even able to see variations in packing density in the anterior pole due to the curvature.

2D Vertex modeling

Here, we describe the implementation of our two-dimensional vertex model dynamics. The position of the vertex i (as counted from $i = 1$ at the trunk) on the apical side is denoted $X_i^a = (x_i^a, y_i^a)$; similarly $X_i^b = (x_i^b, y_i^b)$ refers to the i -th vertex on the basal side. At the first time of the simulation, apical vertices are equally distributed on the first quadrant of the ellipse with principal axis of length $a = 2.5$ and with minor axis of length $b = 1$, which sets the unit of the 2D vertex simulation; the position of the basal vertices is obtained from the position of the apical vertices by a translation at a distance $e_0 = b/5$ along the normal to the ellipse. The equation of motion of the i -th vertex on the basal side reads:

$$X_i^b(t+1) = X_i^b(t) + (F_i^b/\nu)\Delta t$$

where F_i^b is the force acting on the vertex, $\nu = 1$ is a friction coefficient and $\Delta t = 1$ is the time step. Following a standard approach^{5,6}, we derive the expression of the forces by differentiation of the effective energy E (defined in the main text)

$$F_i^b = \frac{\delta E}{\delta X_i^b}$$

Applying a similar method for vertices on the apical side leads to set of apical vertices positions $X_i^a(t+1)$. To model the binding of apical edges to the vitelline membrane, the apical vertices position is projected on the confining ellipse. After evaluation of the angle

$$\theta = \text{atan2}[y_i^a(t+1), x_i^a(t+1)]$$

we perform the projection on the ellipse through the following expression:

$$x_i^a(t+1) = \frac{ab \cos \theta}{\sqrt{b^2 \cos^2 \theta + a^2 \sin^2 \theta}}, \quad y_i^a(t+1) = \frac{ab \sin \theta}{\sqrt{b^2 \cos^2 \theta + a^2 \sin^2 \theta}},$$

We stop the simulations when the energy of the cell has converged to its final value.

We emphasize that E should be referred to as an *effective* energy. Indeed, out-of-equilibrium system may not converge to a state of minimal *thermodynamic* energy. During cellularization, forces are essentially generated within the cortex, which is a fundamentally out-of-equilibrium system. Defining an effective energy should only be thought as a convenient method to express cellular forces.

3D Vertex modeling

Motivation - The 2D vertex model previously used to predict the cell skew cannot be directly applied to describe T1-transitions, since in the model the apical and basal should not vanish. In the absence of skew, the cell-cell membrane direction is aligned with the normal to the apical surface, in which case we do not expect growth to significantly affect the dynamics of the apical vertices within the tangential plane of the apical surface. However, we expect the cell growth force to contribute all the more significantly to the tangential dynamics of apical vertices that there is more skew. This observation motivated us to develop a 3D vertex model to test the interplay between T1 transitions and geometric constraints.

Geometry We performed simulations in regions corresponding to approximately 200 cells, which corresponds to a limited portion of interest of the *Drosophila* embryo. To model the constraints imposed

by the yolk and by the vitelline membrane, we set the rule that vertices should move on the following 2D surfaces: an ellipsoid cap (corresponding to the head) or to an arc portion of cylinder (corresponding to the trunk). This requirement is implemented through a step-by-step normal projection of each vertices position to its closest point on the apical/basal surface. More precisely, at the head, the apical surface is an ellipsoid cap of axes $(a_{\text{apical}}, a_{\text{apical}}, b_{\text{apical}})$ and the basal surface is an ellipsoid cap of axes $(a_{\text{apical}} - h, a_{\text{apical}} - h, b_{\text{apical}} - h)$, where h is a characteristic cell depth at a given time during the cellularization process (see Figure 8H). The unit length in simulation corresponds to a typical apical cell junction length, hence we define the conversion rule: 1 unit = 5 μm . To model the constraint exerted by the rest of the tissue outside of the region of interest, the vertices at the border of the region of interest are fixed to their initial position.

Measure of face area Cells are represented by their apical and basal faces, i.e. the two set of trilateral junctions that are on the apical and basal surfaces. To measure each face area, we divide those apical and basal cell faces into elementary triangles that are defined by two consecutive vertices and the face barycenter. As illustrated in Supplemental Figure S8D, the area of such elementary triangle A_T between the face barycenter $G = (x_G, y_G, z_G)$ and the vertices $B = (x_B, y_B, z_B)$ and $C = (x_C, y_C, z_C)$ is given by

$$A_T = \frac{1}{2} \sqrt{\begin{vmatrix} x_G & x_B & x_C \\ y_G & y_B & y_C \\ 1 & 1 & 1 \end{vmatrix}^2 + \begin{vmatrix} y_G & y_B & y_C \\ z_G & z_B & z_C \\ 1 & 1 & 1 \end{vmatrix}^2 + \begin{vmatrix} z_G & z_B & z_C \\ x_G & x_B & x_C \\ 1 & 1 & 1 \end{vmatrix}^2}$$

where $|M|$ represents the determinant of a matrix M . To obtain the gradient of the area with respect to each vertex, we make use of Jacobi's formula, which states that the derivative of the determinant of the matrix is equal to the transpose of its comatrix $\text{adj}(M)$:

$$\frac{\partial |M|}{\partial M_{ij}} = \text{adj}^T(M)_{ij}$$

Initialization and dynamics The final cell configuration is obtained through the three following steps:

1. We generate a 2D-network of vertices on a flat surface, which we then project on the *apical surface*: that is either an ellipsoid cap (head) or a portion of cylinder (trunk). We then let the apical network relax until convergence of the energy

$$E = \sum_c \beta_A^a (A_c^a - A_0^a) + \beta_P^a (P_c^a - P_0^a)$$

where β_A^a, β_P^a represent the compressibility in the apical area and perimeter respectively. A_0^a, P_0^a represent the target perimeter and area of the apical cell face perimeter respectively. We assume that $A_0^a = \langle A_c^a(0) \rangle$ where $\langle A_c^a(0) \rangle$ is the mean apical face area at $t = 0$. We further assume that $P_0^a = 0.9 \langle P_c^a(0) \rangle$ where $\langle P_c^a(0) \rangle$ corresponds to the expected perimeter for a tissue of hexagonal cells of area $\langle A_c^a(0) \rangle$. The ratio $P_0^b / \langle P_c^b(0) \rangle = 0.95$ is weakly different from 1 in order to generate a weakly tense apical network⁶.

2. We perform a normal projection of the final configuration of the apical network onto the basal surface. We then let the basal network relax until convergence of the energy

$$E_{\text{basal}} = \sum_c \beta_A^b (A_c^b - A_0^b) + \beta_P^b (P_c^b - P_0^b)$$

where we assume that $A_0^b = \langle A_c^b(0) \rangle$ where $\langle A_c^b(0) \rangle$ is the mean basal cell area at $t = 0$. We further assume that $P_0^b = 0.85 \langle P_c^b(0) \rangle$ where $\langle P_c^b(0) \rangle$ corresponds to the expected perimeter for a tissue of hexagonal cells of area $\langle A_c^b(0) \rangle$. The ratio $P_0^b / \langle P_c^b(0) \rangle = 0.85$ is significantly different from 1 to generate a tense hexagonal basal network⁶, which is expected due to the basal actomyosin rings.

3. In the last phase, which we call the *cell depth relaxation phase*, we fix the position of the basal vertices (i.e. corresponding to a robust tense basal network) while apical vertices move until convergence of the energy:

$$E = \sum_c \beta_A^a (A_c^a - A_0^a) + \beta_P^a (P_c^a - P_0^a) - \alpha_L (L_0 - L_c)$$

where

- (i) the first term on the right hand side represents the strength generated by the cell-cell lateral membrane growth: L_c is the cell depth, i.e. the distance between its apical and basal face barycenter (see Figure 8G); $\alpha_L > 0$ represents the compressibility in the cell depth with respect to a control depth $L_0 = h$. We consider the target cell depth L_0 as fixed during the cell junction relaxation phase. This is motivated by the fact that the total cellularization process is relatively long (approx. 45 min) compared to a typical cell junction relaxation time (typically around 1 min).
- (ii) the second and third terms represent the cell resistance to deformation: A_c^a and P_c^a are the initial cell area and perimeter; A_0^a , P_0^a are the target cell area and perimeter; A_0^b , P_0^b are equal to their value defined in step 2.

Results: The growth force is oriented towards the outward of the apical surface, since the cell depth after initialization is smaller than the target value: $L_c < L_0 = h$. As expected, in the absence of growth force ($\alpha_L = 0$) the apical vertices do not move during the cell depth relaxation phase. Setting $\alpha_L = 20$, we observe a reduction in the length of cell junctions that are oriented towards the head pole. When the cell depth h exceeds 4 units = 20 μm , the length of such cell junctions is critically reduced, eventually reaching the threshold length $\Delta = 0.25 = 1.25 \mu\text{m}$ for T1s. These T1s are located at an anterior-posterior distance equal to 4 units = 20 μm . Therefore, the localization of these T1s appear to be correlated with that of the maximum skew angle (see Supplemental Figure S8H). The orientation of T1s could be determined by the gradient of the cell skew. We will elaborate further on the underlying mechanical aspects in a following publication.

We provide in Table S1 the parameter values used to obtain the results presented in Figure 8G (main text). With this set of parameters, the skew angle measured in simulations (see Supplemental Figure S8D) is in good agreement with the experimental measurement (see Figure 6B). We also observe that the minimal apical cell junction length decreases as the cell depth h increases, when $h > 2$ units = 10 μm (see Supplemental Figure S8H). The junction length reaches our threshold length $\Delta = 0.20 = 1 \mu\text{m}$ for triggering T1 transition at a cell depth $h = 4 = 20 \mu\text{m}$.

As shown in the Supplementary Movie 6, the observed pseudo-T1s lead to a cell configuration that is only transiently stable: the stable final configurations appear to correspond to hexagonally packed cells. We will further explore the parameter phase space to investigate whether other cell packing configurations can reach a stable steady state in a following publication.

General					Basal				Apical			
Number of cells	r	dt	α_L	Δ	β_P^b	β_A^b	A_0^b/A_{mean}^b	P_0^b/P_{mean}^b	β_P^a	β_A^a	A_0^a/A_{mean}^a	P_0^a/P_{mean}^a
211	13.5	0.005	20	0.25	1	5	1	0.85	0.5	2	1	0.9

Table S1 – Values of the parameters used to obtain the results in Figure 8D and Supplemental Figure S8G-H.

Supplementary References

1. Hara, Y., Shagirov, M. & Toyama, Y. Cell Boundary Elongation by Non-autonomous Contractility in Cell Oscillation. *Curr Biol* 1–10 (2016). doi:10.1016/j.cub.2016.07.003
2. Sommer, C., Straehle, C. & Kothe, U. ilastik: Interactive learning and segmentation toolkit. *IEEE International Symposium on Biomedical Imaging* (2011).
3. Roerdink, J. B. T. M. & Meijster, A. The Watershed Transform: Definitions, Algorithms and Parallelization Strategies. *Fundamenta Informaticae* **41**, 187–228 (2000).
4. Dunn, F. & Parberry, I. *3D math primer for graphics and game development*. (Wordware Publishing, 2015).
5. Fletcher, A. G., Osterfield, M., Baker, R. E. & Shvartsman, S. Y. Vertex Models of Epithelial Morphogenesis. *Biophys J* **106**, 2291–2304 (2014).
6. Farhadifar, R., Roper, J. C., Aigouy, B., Eaton, S., & Julicher, F. (2007). The Influence of Cell Mechanics, Cell-Cell Interactions, and Proliferation on Epithelial Packing. *Current Biology*, 17(24), 2095–2104